



Parameterization on Fructose-Stabilized Silver Nanoparticle Synthesis by Non-thermal Atmospheric Pressure Helium Plasma Jet

Jirapong Sornsakdanuphap, Khuanjarat Choengpanya and Chanthana Susawaengsup
Program in Basic Science, Maejo University (Phrae Campus), Phrae, Thailand

Lueacha Tabtimmai
Department of Biotechnology, Faculty of Applied Science, King Mongkut's University of Technology North Bangkok, Bangkok, Thailand

Kiattawee Choowongkomon*
Department of Biochemistry, Faculty of Science, Kasetsart University, Bangkok, Thailand

* Corresponding author. E-mail: kiattawee.c@ku.th DOI: 10.14416/j.asep.2024.09.010
Received: 22 May 2024; Revised: 5 July 2024; Accepted: 5 August 2024; Published online: 13 September 2024
© 2024 King Mongkut's University of Technology North Bangkok. All Rights Reserved.

Abstract

The fructose stabilized silver nanoparticles (FRU-AgNPs) synthesis is comparatively studied by defining the experimental parameters such as plasma jet device configuration, AgNO₃ concentration, plasma treatment time and fructose stabilizer concentration. In this research, there are four types of plasma jet device configurations (C1–C4). The plasma treatment time is varied in a range of 10 to 30 minutes. Fructose concentration is varied to be 5, 10, 20 and 40 mM. The helium gas is used to generate non-thermal atmospheric-pressure plasma. The plasma jet device is operated by a sinusoidal power supply at a repetition frequency of approximately 1 MHz. The input electrical power for plasma generation is about 30 W. The formation and stability of AgNPs are characterized by surface plasmon resonance (SPR) absorbance peak from ultraviolet-visible (UV-Vis) spectrophotometer. The absorbance peaks of AgNPs are found in the range of 400 to 420 nm. According to the dynamic light scattering (DLS) technique, the hydrodynamic sizes of AgNPs are in the range of 15 to 40 nm. The AgNPs show anti-bacterial activity against *Escherichia coli* with an average inhibition zone of 8.87 ± 0.55 mm. Based on the highest yield of AgNPs, optimal parameters are found to be C3, plasma treatment time of 30 min, AgNO₃ concentration of 1–2 mM and fructose concentration of 40 mM.

Keywords: Fructose-stabilized silver nanoparticle, Helium plasma jet, Non-thermal atmospheric pressure plasma, Plasma jet configurations

1 Introduction

In the biomedical field, silver nanoparticles (AgNPs) are well-known substances utilized for disinfecting various microorganisms because it has high inhibiting and killing effects. AgNPs have been widely used during the COVID-19 pandemic that caused more than 1.3 million deaths reported by the World Health Organization (WHO) in 2022 [1]. Besides application in the biomedical field, AgNPs can be applied in agricultural and environmental fields, for instance,

they can promote seed germination, nano-pesticide [2] and remove dye from wastewater [3]. AgNPs can be synthesized by various methods such as biological, chemical, physical, or even hybrid methods such as chemical reduction from natural plant extracts [4], reduction from chemicals such as NaOH, trisodium citrate dehydrate [5], pulse laser ablation [6], a blend of silver nitrate and carboxymethyl chitosan with microwaves-assistance [7]. Although there are many ways to synthesize AgNPs, it is still needed to find a more rapid and green synthesis, with low energy



consumption, and low-cost production. As mentioned above, the non-thermal atmospheric pressure plasma technique is one of a promising option because it generates no toxic to the environment and has less energy consumption with electrical power in a range of 10–100 W. Also, there are some research employing non-thermal atmospheric pressure plasma-liquid interface technique for AgNP synthesis and it has been applied for efficient antimicrobial activity [8]–[11] or even photocatalytic activity [12]. Interestingly, it is reported that AgNPs are synthesized within a few minutes by non-thermal atmospheric pressure plasma processing [13]. Even more, it has the feasibility to scale up to the industry level. Non-thermal plasma is defined as gas discharged into a plasma state, in which electron temperature in atmospheric pressure is characterized in a range of 1–3 eV depending on working gas species [14], [15]. For non-thermal plasma, the electron has a higher temperature than that of other species such as positively charged ions, reactive radicals, and excited atoms in which their temperatures are nearly at ambient gas temperature. Non-thermal plasma is a good candidate for efficient nanoparticle synthesis. However, it is partially ionized gas with electron density around 10^{12} – 10^{15} cm^{-3} under atmospheric pressure chemical reaction [16]. This might be the drawback in some applications which require relatively high electron density for chemical reactions. Normally, the synthesis of AgNPs requires a substance to stabilize its structure since it either easily redissolves in solution or agglomerates within several hours. The substances commonly used for AgNP stabilization could be several types such as the polymer, anionic molecule, polysaccharide, or even polysaccharides from plant extract for instance polyvinylpyrrolidone (PVP), citrate [17], chitosan [18] and polysaccharides from *Leucaena leucocephala* seed [19], respectively. However, from a biomedical perspective, fructose is an interesting substance for stabilization because it can trigger chemotaxis of pathogenic bacteria [20], and good biocompatibility with human cells [21]. Moreover, it is available at a low cost, therefore in this study, fructose is chosen as a candidate for AgNP stabilization. Although the formation of AgNPs has been well characterized, its anti-microbial mechanism is yet to be elucidated. Based on bioinformatic analysis, it is suggested that AgNPs might attach to the

bacterial surface, and destabilize the cell wall and membrane followed by induction of intracellular reactive oxygen species (ROS) causing oxidative stress [22], [23]. In addition, it is reported that anti-bacterial activity of AgNPs is more effective in Gram-negative bacteria because this kind of bacteria has a thinner peptidoglycan layer in comparison to that of Gram-positive bacteria. Thus, it is conducive to more penetrations into gram-negative bacterial cells [24].

Based on a non-thermal atmospheric pressure plasma jet discharge system, this current research is focused on how experimental parameters affect AgNP synthesis by parameterization of jet device configuration, plasma treatment time, AgNO_3 concentration, and fructose stabilizer concentration. Since, the characteristics of electron temperature and electron density of non-thermal atmospheric pressure plasma are in a range of 1–3 eV and 10^{12} – 10^{15} cm^{-3} as mentioned earlier. These characteristics might define the chemical reaction to form AgNPs with particular properties, e.g., size or density in the solution. Therefore, the parameterization is beneficial to estimate optimal synthesis conditions based on a non-thermal atmospheric pressure plasma jet discharge system. Also, the parameterization would help to understand a limitation of a non-thermal atmospheric pressure plasma jet discharge system and that limitation might be further developed. When optimal synthesis condition regarding an arbitrary unit volume of solution is well defined, the feasibility for larger scale or industrial level application can occur. Generally, non-thermal atmospheric pressure plasma can be scaled up by designing multiple or arrayed plasma jets as reported in some research [25], [26]. However, for AgNP synthesis on a larger scale, multiple plasma jets can be applied on separated wells of solution in a tray. For more precision on the x-y-z movement of plasma jet and treatment time duration, these plasma jets can be assembled with stepping motors, servo motors, conveyor belts and microcontrollers by supporting more power supply. Even though the plasma jet machine for AgNP synthesis can be assembled and operated. The reproducibility, stability, and worthiness of plasma jet machines should be for further study. Moreover, the anti-bacterial activity of AgNPs is also investigated. The results from current research will give more information for biomedical and agricultural applications of AgNPs.

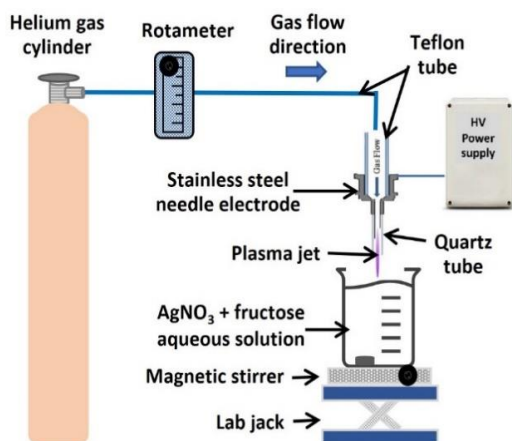


Figure 1: Schematic diagram of plasma jet discharge system for synthesis of fructose-stabilized silver nanoparticle (FRU-AgNPs).

2 Materials and Methods

2.1 The plasma jet discharge system and jet device configurations

The plasma jet device is made from a stainless-steel syringe needle inserted into a quartz glass tube. It is noted here that the quartz glass tube used in our experiment has a relatively wide diameter in comparison to the quartz glass tube used in the common plasma jet. This reduces gas velocity impinging on the surface of liquid precursor ($\text{AgNO}_3 + \text{fructose}$ in aqueous solution) that can prevent liquid splashing inside a glass tube. For this reason, inner and outer diameters of quartz glass tube are set to be 5 mm and 7 mm, respectively. Its length and thickness are 40 mm and 1 mm, respectively. The distance between a stainless steel syringe needle tip and a nozzle of quartz glass tube (plasma jet nozzle) is 10 mm to prevent liquid splashing inside the syringe needle. The top end of a syringe needle is fitted to a teflon tube. Helium gas with purity of 99.9% is fed to teflon tube and is passed through the syringe needle. The syringe needle as a powered electrode is connected to a high voltage terminal of power supply that can generate sinusoidal wave with frequency of approximately 1 MHz as shown in (Figure 1).

For comparative study, there are four types of jet device configuration. The first jet device configuration is a plasma jet nozzle positioned 3 mm above liquid precursor surface in which the plasma plume is customized to be the longest filament discharge Figure 2(C1). The

second jet device configuration is a plasma jet nozzle positioned 3 mm above the liquid surface with fog-like discharge Figure 2(C2). The third and fourth jet device configurations (Figure 2(C3) and (C4)) are plasma jet nozzles positioned just below the liquid surface in which the plasma plume is long filament-like discharge and fog-like discharge, respectively. It is noted that the bubbles below the liquid surface can be formed in both Figure 2(C3) and (C4). Additionally, the flow rates of helium gas are adjusted by a rotameter at 0.8, 0.2, 0.4 and 0.2 liters per minute (LPM) for Figure 2(C1)–(C4), respectively. In all experiments, the total volume of liquid precursor is fixed at 3 mL inside a beaker of 10 mL and stirred by a magnetic bar. In addition, the parameter of input electrical power is about 30 W. Here, fructose is used as a stabilizing agent. The plasma treatment time is in a range of 10 to 30 min depending on each study.

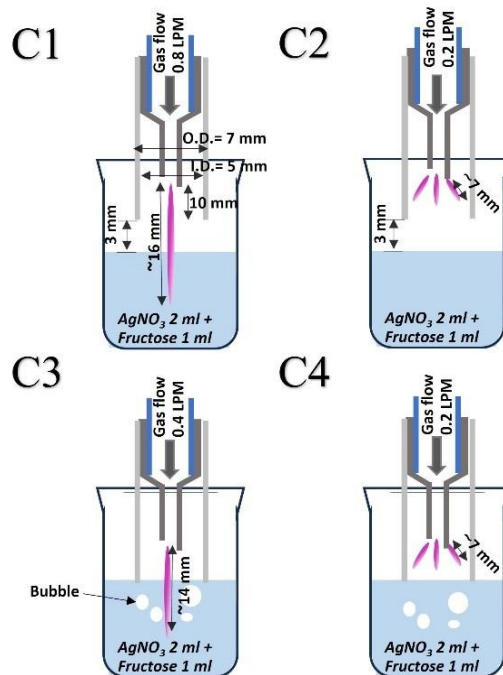


Figure 2: Illustration of four types of plasma jet device configurations. The plasma jets of (C1) and (C2) are positioned above liquid precursor surface. The distance between liquid precursor surface and the jet nozzle is fixed to be 3 mm. The plasma jets of (C3) and (C4) are positioned just below the liquid precursor surface in which bubble formation can be observed. The four configurations are designed to comparatively study the synthesis efficiency, formation, and stability of AgNPs. Plasma treatment time is fixed at 10 min.



2.2 Reagents and solutions

AgNO₃ and fructose are of analytical grades. The stock solutions of AgNO₃ or 40 mM fructose are prepared in ultra-pure water. The volume ratio of AgNO₃ : fructose used in all experiments is 2 : 1. The mixture between AgNO₃ and fructose before plasma treatment is defined as a liquid precursor.

The comparison of the efficiency of the plasma jet device configurations Figure 2(C1)–(C4) on AgNP synthesis is carried out. Two milliliters of 1 mM AgNO₃ are mixed with 1 mL of 40 mM fructose in a 10 mL beaker before performing plasma treatment with each plasma jet device configuration. The plasma treatment time is fixed at 10 min.

The effect of plasma jet device configurations Figure 2(C1)–(C4) on the formation and stability of AgNPs are also studied, AgNO₃ concentrations are varied to be 0.125, 0.25, 0.5, and 1 mM. Two milliliters of each concentration of AgNO₃ are mixed with 1 mL of 40 mM fructose before performing plasma treatment for 10 minutes.

The effects of relatively high concentrations of AgNO₃ and plasma treatment time on the surface plasmon resonance (SPR) absorbance peak of AgNPs are also studied. Two milliliters of each concentration of AgNO₃ at 1, 2, 4 and 8 mM is mixed with 1 mL of 40 mM fructose before performing plasma treatment. The plasma treatment time is varied to be 10, 20 and 30 min. For a study on the effect of fructose stabilizer concentration on the absorbance peak of AgNPs, 2 mL of 2 mM AgNO₃ is mixed with 1 mL of various fructose concentrations at 5, 10, 20 and 40 mM.

2.3 Determination of plasma species

Optical emissions spectroscopy (OES) is used to determine plasma species in plasma jets. The spectra are obtained by the spectrometer of Avantes Avaspec-3648. The optical aperture is positioned 5 mm above the jet nozzle without beneath the solution.

2.4 Characterization of formation and stability of FRU-AgNPs

The ultraviolet-visible (UV-Vis) spectroscopy is the technique used to characterize AgNP formation by determining the spectral peak of SPR. The absorption spectra are acquired by a Varian Cary 50 spectrophotometer in the spectral range from 350 to 750 nm. The scanning speed is 20 nm/s and the step is

0.25 nm. The stability of AgNPs is monitored by observing the shift of SPR peak with respect to time.

2.5 Particle size distribution of FRU-AgNPs

The hydrodynamic size distribution of FRU-AgNPs is determined by Dynamic Light Scattering (DLS) technique by using Malvern Zetasizer Nano ZS90 and the size distribution by intensity profiles is acquired by Zetasizer software version 7.11. The polydispersity index (*PDI*) can be determined by the parameters of mean diameter and standard deviation of diameter.

2.6 Anti-bacterial activity against *Escherichia coli*

The anti-bacterial activity of FRU-AgNPs against Gram negative bacteria, *E. coli*, is performed by disc diffusion method. The nutrient agar (NA) plate is inoculated with 0.5 McFarland unit of *E. coli* culture. Two milliliters of 1 mM AgNO₃ are mixed with 1 mL of 40 mM fructose, and the solution is subjected to plasma treatment for 20 min. After that, the FRU-AgNPs are purified by centrifugation at 12,000 rpm for 20 min and washed with 13.33 mM fructose. The FRU-AgNPs are resuspended in 15 µL 13.33 mM fructose before dropping onto the 6-mm sterile filter paper disc. The 15 µg of antibiotic streptomycin is used as a control. The plate is incubated at 37 °C for 16–18 h, then the growth inhibition zone (clear zone) is measured.

3 Results and Discussion

3.1 Plasma species composition

In this study, optical emissions spectroscopy (OES) is a method to identify plasma species inside our helium plasma jet. The measuring spectral range is from 250 to 800 nm. Most species found in our plasma jet are excited second positive system of N₂, excited He, excited first negative system of N₂⁺, OH radical, atomic H, atomic O as shown in (Figure 3). These plasma species found in our study are consistent with those reported by using the same atmospheric pressure helium plasma [27], [28]. It is noted here that the OH radical peak is found at 309 nm, H-alpha is found at 657 nm, H-gamma is found at 434 nm and atomic oxygen is found at 777 nm. Furthermore, second positive system of N₂ is found in a range from 316 to 405 nm with dominant peaks of 337 and 358 nm. The dominant peaks of the first negative system of N₂⁺ are

found at 391 and 427 nm. The dominant peaks of helium are found at 354 and 706 nm. It should be noted here that OH radical is mainly caused by electron impact on water molecules.

To simplify and help to visualize in the latter discussion, the main chemical reactions forming Ag⁰ monomer and subsequently becoming AgNPs are proposed and summarized as shown in (Table 1). In (Table 1), the main chemical reactions are divided into

4 steps. Firstly, the electrons collide with water to form OH and H. Secondly, the reactive H reacts with Ag⁺ to form Ag⁰ monomer and H⁺ that H⁺ is the main cause for solution pH decrease. Thirdly, OH is responsible for the formation of secondary reducing species as H₂O₂ and aldehyde. Fourthly, long-lived H₂O₂ and aldehyde react with Ag⁺ to form further Ag⁰ monomer.

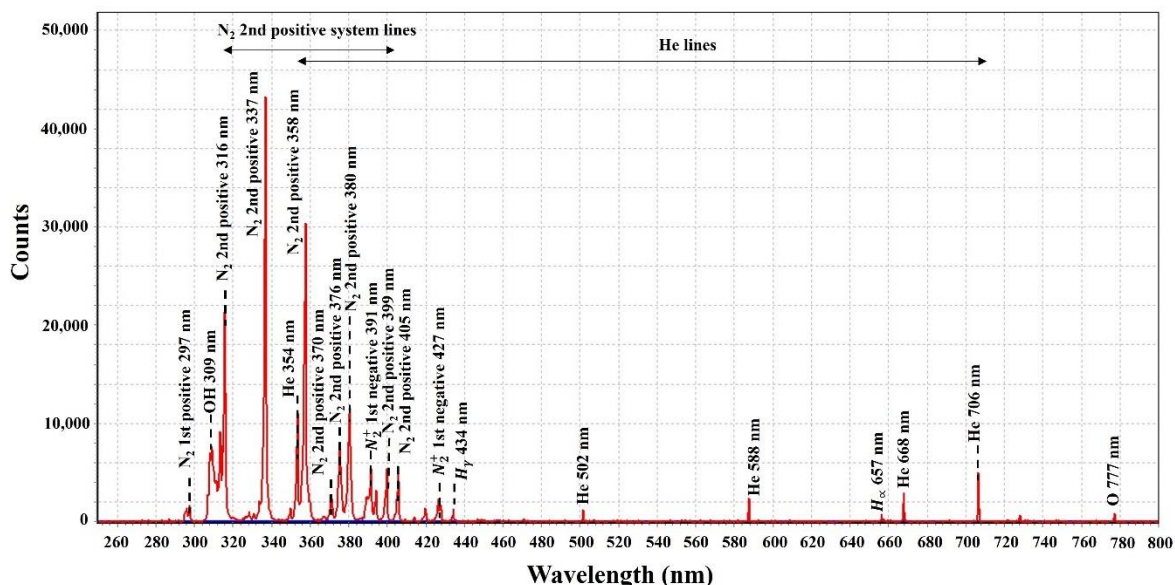


Figure 3: Optical emission spectra of helium plasma jet without beneath solution. The spectral range is from 250 to 800 nm. The optical aperture is positioned 5 mm above the jet nozzle. The flow rate is fixed at 0.4 LPM.

Table 1: Proposed main chemical reactions of plasma species for Ag⁰ monomer formation

Steps and Explanation	Chemical Reactions
Step1: (electron impact on the dissociation of water)	$e^- + H_2O \rightarrow OH + H + e^-$
Step2: (Ag+ reduction by electron and atomic hydrogen)	$Ag^+ + e^- \rightarrow Ag^0$ $Ag^+ + H \rightarrow Ag^0 + H^+$
Step3: (Formation of secondary reducing species as H ₂ O ₂ and aldehyde)	$OH + OH \rightarrow H_2O_2$ $fructose + OH \rightarrow R - CHO$
Step4: (Ag+ reduction by secondary reducing species as H ₂ O ₂ and aldehyde)	$Ag^+ + H_2O_2 \rightarrow Ag^0 + O_2 + 2H^+$ $2Ag^+ + H_2O + R - CHO \rightarrow 2Ag^0 + R - CO_2H + 2H^+$

3.2 Effect of jet configurations on the efficiency of FRU-AgNPs synthesis

In this experiment, the plasma discharge features are classified to be filament-like discharge and fog-like discharge as shown in (Figure 4(a) and (b)), respectively. To generate a plasma jet as fog-like discharge, the gas flow is limited not to be greater than 0.2 LPM based on our plasma jet. It also can be seen in (Figure 4) that plasma in filament-like discharge has

an intensity slightly higher and penetration deeper into liquid precursor than those of plasma in fog-like discharge. Based on our plasma jet, plasma in filament-like discharge can be customized to be longest when gas flow is set to be about 0.8 LPM as shown in C1. However, to reduce liquid splashing inside a glass tube, the gas flow rate of C3 is set to be about 0.4 LPM.

To compare the efficiency of C1–C4, 1 mM AgNO₃ is mixed with 40 mM fructose. After each jet

configuration is operated for 10 min, C3 has the highest absorbance peak of about 0.31 indicating a relatively high density of the AgNPs at a detected peak of 410 nm as shown in (Figure 5). The wavelength of this peak is slightly lower (blue shift) than those of C1, C2 and C4 which are detected at 416, 416 and 413 nm, respectively. The blue shift observation of C3 is due to the average particle size of AgNPs becoming smaller. This is oppositely explained as a red shift reported in the literature [29].

This reason is attributed to the flux entering the solution of strong reducing solvated electrons (e_{aq}^-) of C3 is higher than those of C1, C2 and C4. Since e_{aq}^- of C3 can be found in relatively high density in solution, it causes a faster rate of nucleation of AgNPs and consequently, the particles become smaller [30]. Therefore, in our current study, C3 is chosen as a model plasma jet configuration as it has relatively high efficiency to generate a greater density of AgNPs. On the other hand, the absorbance peaks observed in C1 and C2 are lower than those of C3 and C4 as shown in (Figure 5) due to the impact of distance between the jet nozzle and the surface of the liquid precursor.

This considerably affects plasma electron penetration into the solution as a longer distance leading to a lower flux of plasma electrons entering the solution. In addition, C2 has a significantly lower absorbance peak in comparison to that of C1. This might be due to the huge difference in flow rate between C1 and C2 as they are 0.8 and 0.2 LPM, respectively. Based on our plasma jet in which the diameter of the jet nozzle is quite large, a flow rate of 0.2 LPM might not be laminar flow. Also, helium is a low dense gas, which causes the gas to streamline rapidly to float up and sweep more plasma electrons away from a liquid interface by convection. The experimental conditions and results for C1–C4 are summarized in (Table 2).

Table 2: Experimental conditions and results for evaluation of the effectiveness of jet configurations.

Jet Configurations/Conditions	C1	C2	C3	C4
Distance from jet nozzle to liquid (mm)	3	3	0	0
Gas flow rate (LPM)	0.8	0.2	0.4	0.2
Treatment time (min)	10	10	10	10
AgNO ₃ concentration (mM)	1	1	1	1
Fructose concentration (mM)	40	40	40	40
AgNO ₃ / Fructose (mL)	2/1	2/1	2/1	2/1
Absorbance peak	0.18	0.11	0.31	0.23
Wavelength at absorbance peak (nm)	416	416	410	413

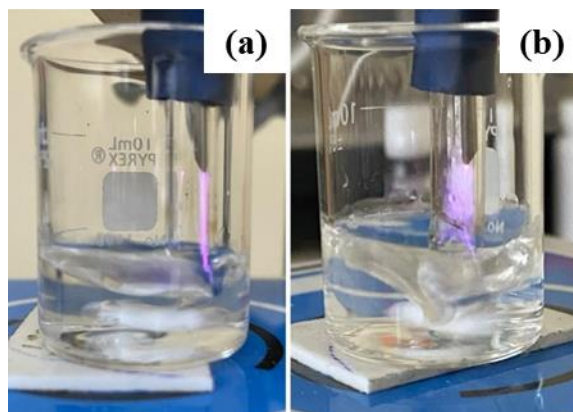


Figure 4: Photograph of plasma jet discharge shows (A) filament-like discharge above liquid precursor surface as set up to be C1 (B) fog-like discharge above liquid precursor surface as set up to be C2.

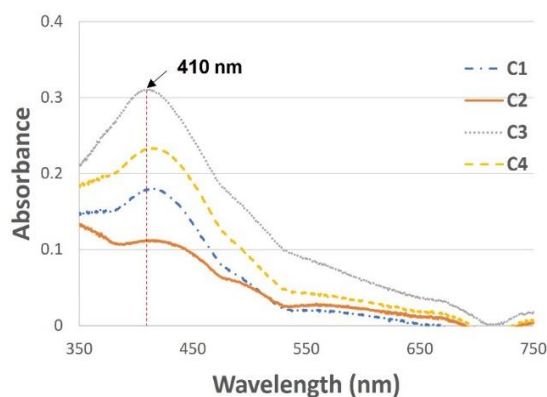


Figure 5: UV-Vis absorption spectra of plasma jet configuration of C1 to C4. The liquid precursor of each configuration is prepared by mixing 2 mL of 1 mM AgNO₃ with 1 mL of 40 mM fructose under a fixed plasma treatment time of 10 min.

3.3 Effect of jet configurations on FRU-AgNPs formation and stability

After plasma treatment for 10 min, the AgNPs formations from C1, C2, C3 and C4 can be observed from the SPR absorbance peaks (Figures 6–9). However, all absorbance peaks (abp) in Figures 6–9 are low in which they stay in a range of 0.1 to 0.3. The full width at half maximum ($FWHM$) values of C1 to C4 are also greater than 160 nm. Since, a parameter of $\frac{abp}{FWHM}$ can be used to roughly interpret size distribution in which $\frac{abp}{FWHM}$ less than 0.003 is implied to be

polydisperse morphology as AgNPs synthesized via Lee-Meisel method reported in the literature [31]. Because the values of $\frac{abp}{FWHM}$ obtained from our jet configurations of C1 to C4 are about 0.002, the AgNPs from these configurations under 10 min of plasma treatment are interpreted as polydisperse nanoparticles. It is noted that the formation and stability of AgNPs are firstly studied on relatively low concentrations of AgNO_3 , which are 0.125, 0.25, 0.5 and 1 mM. Here, 1 mM is supposed to be the concentration line where it is used to separate between high and low concentrations of species in solution since solvated electron concentrations are generally found to be around 1 mM as reported in the plasma-liquid interface at atmospheric pressure [32]. For the jet nozzles above the liquid surface (C1 and C2), it can be observed that absorbances of C1 and C2 are likely to remain unchanged over a period of 1 h after plasma treatment where AgNO_3 concentrations are lower than

0.25 mM. The increasing trend of about 20 min and decreasing trend of about 40 min of absorbance peaks of C1 at AgNO_3 concentrations of 0.5 and 1 mM are observed as shown in Figure 6. These increasing trends of absorbance peaks of C1 might be due to the remaining reducing agent such as H_2O_2 or aldehyde. H_2O_2 is a long-lived ROS induced initially by plasma electron collision with water whereas aldehyde is converted from fructose by plasma effect [32]. It also can be seen that the increase in absorbance peaks from 0–20 min of C1 after plasma treatment is about two times as shown in Figure 6. In Figure 7, over a period of 1 h after plasma treatment, the absorbances of C2 seem likely to remain unchanged for all AgNO_3 concentrations ranging from 0.125–1 mM. This can be implied that under C2 operation, FRU-AgNPs are quite stable at relatively low concentration of AgNO_3 precursor and 40 mM fructose is considered as a stabilizing condition.

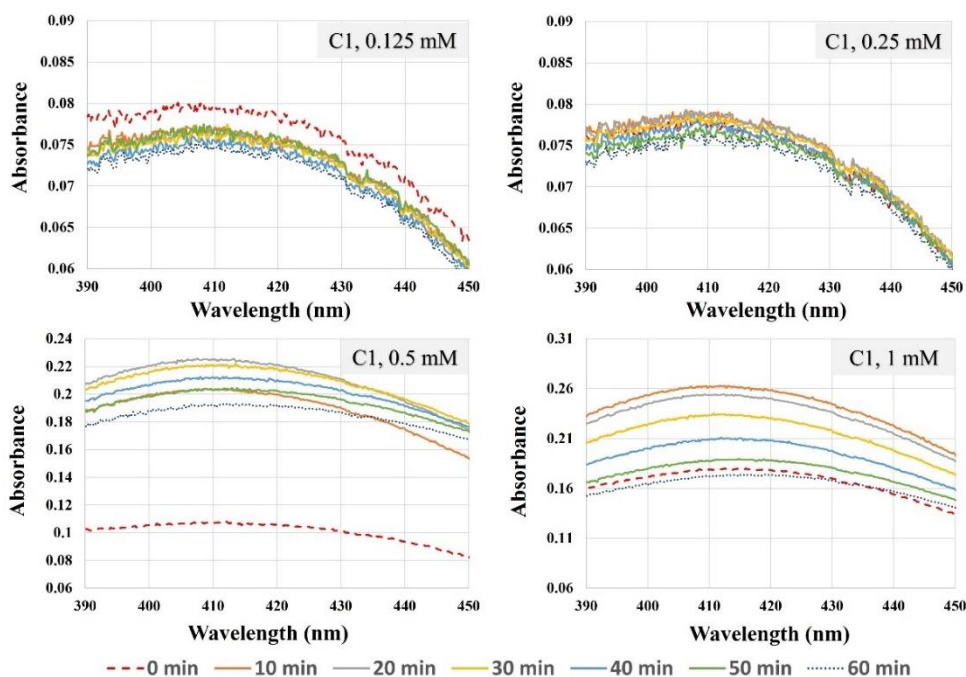


Figure 6: UV-Vis absorption spectra of C1 show formations and stabilities of AgNPs over a period of 1 h at AgNO_3 concentrations of 0.125 mM, 0.25 mM, 0.5 mM and 1 mM.

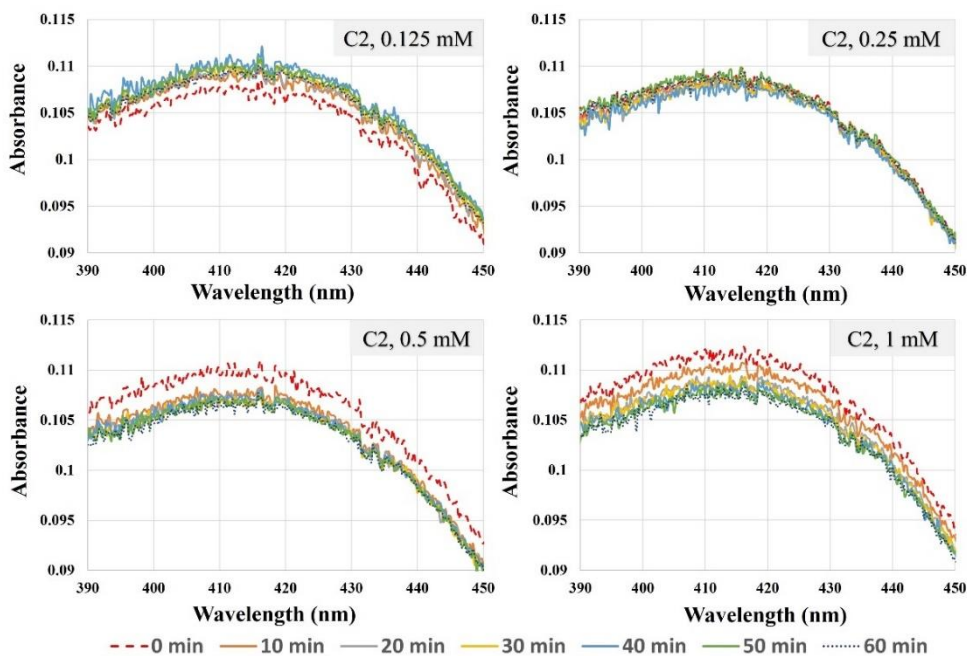


Figure 7: UV-Vis absorption spectra of C2 show formations and stabilities of AgNPs over a period of 1 hour at AgNO_3 concentrations of 0.125 mM, 0.25 mM, 0.5 mM and 1 mM.

In Figure 8 under C3 operation, it can be seen the increasing trend of absorbances of 0.125, 0.25, and 0.5 mM AgNO_3 about 20 min after plasma treatment except it is 10 minutes for 1 mM AgNO_3 . Furthermore, after reaching the maximum value, the absorbances of 0.125, 0.25, and 0.5 mM AgNO_3 show a slightly decreasing trend, except for 1 mM AgNO_3 in which the decreasing trend is faster and larger as shown in Figure 8. From this observation, it seems likely that a higher concentration of AgNO_3 induces a faster decreasing trend that might be related to the initial aggregation of the nanoparticles where the concentration of 40 mM fructose is used as a stabilizer. This initial aggregation is probably due to the accumulation of silver ion residues after plasma treatment in Stern and Diffuse layers as described model in the literature [33]. The H^+ during plasma treatment might also be accumulated in the Diffuse layer. These lead to the decrease in zeta potential absolute value which induces aggregation as described in the literature [33]. In a comparison of C4 to C3, where AgNO_3 concentration is lower than 0.25 mM, the increasing trend of C4 about 40–50 min after plasma treatment until reaching maximum absorbance

takes more time as shown in Figure 9. This is due to lower concentration of plasma induced long-lived species, i.e., H_2O_2 or aldehyde which are responsible for reducing agents of AgNPs after plasma treatment as mentioned earlier. Consequently, the lower concentration of long-lived species of C4 results in a slower chemical reaction rate for AgNPs post-formation. However, when $\text{AgNO}_3 > 0.5$ mM, Ag^+ remaining in solution is more predominant than long-lived species in which this Ag^+ defines faster chemical reaction rate for AgNPs post-formation. Therefore, the increasing trends of C3 and C4 are not much different as they are about 20–30 min for 0.5 mM AgNO_3 and about 10 min for 1 mM AgNO_3 , respectively as shown in Figures 8 and 9. It should be noted here that faster nucleation causes smaller AgNPs. Also, lower wavelength of SPR absorbance peaks from UV-Vis absorption spectra can indicate smaller size of AgNPs as mentioned earlier. Since C3 is deduced to generate relatively higher flux of solvated electron (e_{aq}^-), this promotes faster nucleation and results in smaller nanoparticles as can be observed clearly in a range of 400–405 nm for 0.125 mM AgNO_3 (Figure 10).

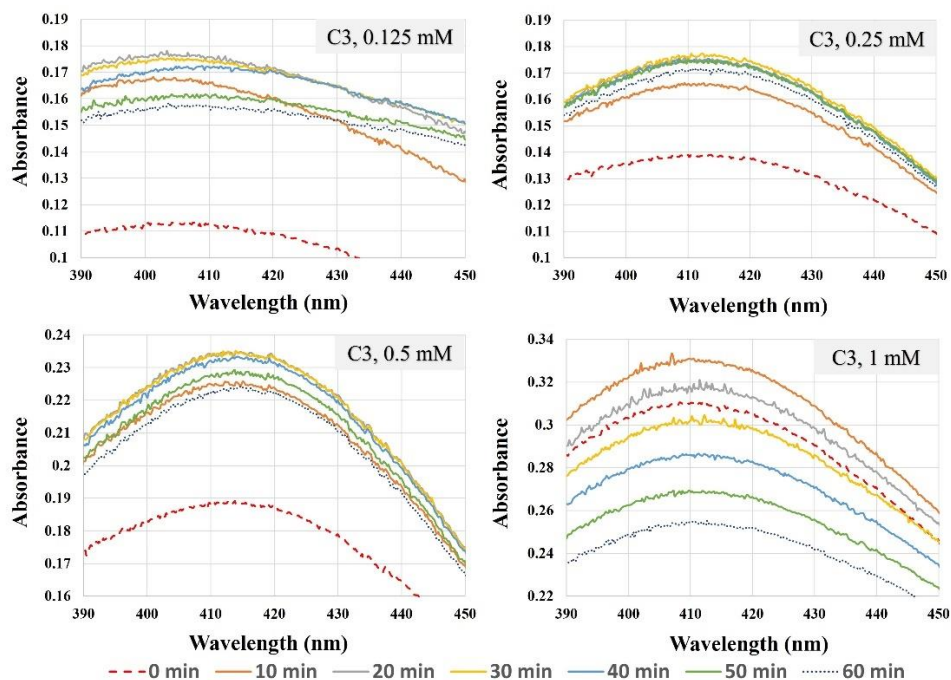


Figure 8: UV-Vis absorption spectra of C3 show formations and stabilities of AgNPs over a period of 1 h at AgNO_3 concentrations of 0.125 mM, 0.25 mM, 0.5 mM and 1 mM.

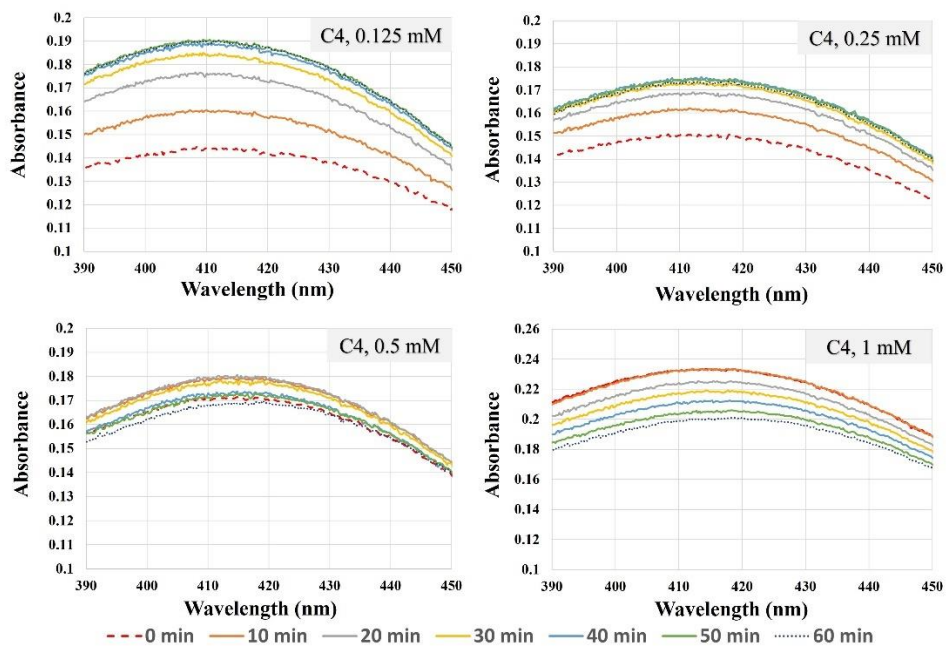


Figure 9: UV-Vis absorption spectra of C4 show formations and stabilities of AgNPs over a period of 1 h at AgNO_3 concentrations of 0.125 mM, 0.25 mM, 0.5 mM and 1 mM.

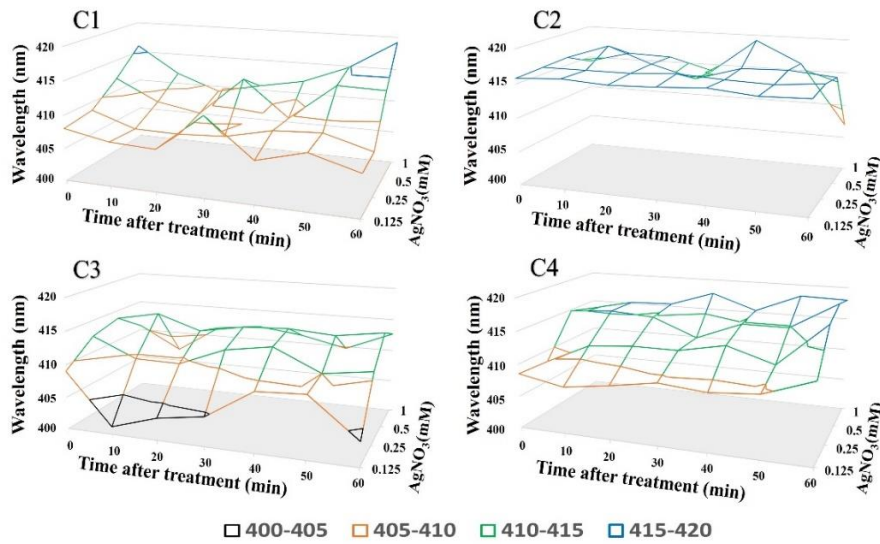


Figure 10: Three-dimensional surface plots of wavelength at absorbance peaks measured by UV-Vis spectroscopy versus times after plasma treatment and AgNO_3 concentrations.

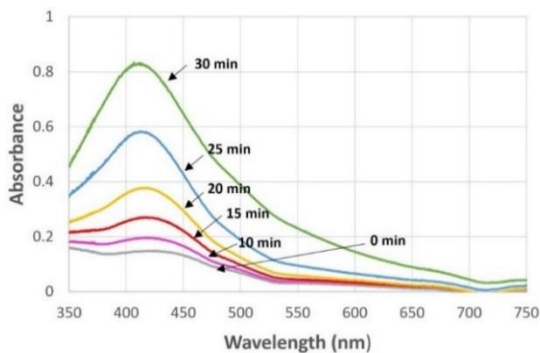


Figure 11: UV-Vis absorption spectra of AgNPs solution measured immediately after plasma treatment for 0, 10, 15, 20, 25 and 30 min that are operated by C3 at 1 mM AgNO_3 and 40 mM fructose.

In Figure 10, it should be noted that the higher concentration of AgNO_3 used, the larger size of AgNPs would become for C1, C3, and C4. Except for C2, the concentration of AgNO_3 does not affect AgNP size. This is probably due to \tilde{e}_{aq}^- generated by C2 is low and nearly the same concentration by using 0.125–1 mM AgNO_3 . Additionally, SPR absorbance peaks from C2 mostly stay in a range of 415–420 nm as shown in Figure 10 indicating a relatively larger size of AgNPs. In an aspect of time evolution after plasma treatment from 0 to 60 min, when $\text{AgNO}_3 \geq 0.5$ mM, it seems likely that AgNPs slowly form larger

size for C1, C3 and C4 as shown in Figure 10. On the other hand, when $\text{AgNO}_3 < 0.5$ mM, the size of the AgNPs is likely to be unchanged for C1, C3 and C4. This can be implied that for $\text{AgNO}_3 < 0.5$ mM, AgNPs have good stability based on C1, C3 and C4 by considering 40 mM fructose as a stabilizing condition. However, for C2, $\text{AgNO}_3 \leq 1$ mM, AgNPs have good stability with a relatively low SPR absorbance peak.

3.4 Effect of plasma treatment time on FRU-AgNPs formation

From C3 operation for plasma treatment times of 10, 15, 20, 25 and 30 min, SPR absorbance peaks measured immediately after plasma treatment are about 0.2, 0.26, 0.38, 0.58 and 0.82, respectively as shown in Figure 11. As expected, this increase is due to more nuclei are generated with more treatment time and growing afterwards to be the AgNPs. Also, for plasma treatment times of 10, 15, 20, 25 and 30 minutes, absorbance peaks are detected at 417, 417, 417, 412 and 407 nm, respectively, that indicates a slight decrease in AgNP size with an increase in plasma treatment time. This result is in good agreement with a report [13] as plasma exposure time increases, the silver nanoparticles become smaller.

In addition, the pH of plasma activated water (PAW) tends to decrease as plasma exposure time increase as reported in some literatures [34], [35]. This

is in good agreement with our experiment that after plasma treatment for 20 min, approximately solution pH decreases from 7.2 to 3.9. With a more acidic environment in PAW, it might be possible that some parts on the surface of AgNPs redissolve to be Ag^+ and combine with e_{aq}^- generated continuously by plasma then become Ag^0 monomers. With sufficient Ag^0 monomers, this generates more nuclei and leads to a smaller size of AgNPs. It also should be noted here that the influence of decreasing pH affects the size to become smaller as reported in the literature [36]. Consistent with the graphs in Figures 11 and 12 show color changes from transparent to pale yellow, confirming a formation of AgNPs stabilized by fructose. As expected, the color becomes browner as plasma treatment time increases. The brown color observed at a plasma treatment time of 30 min is due to higher concentrations of AgNPs. A sequence of color change shown in Figure 12 from 0 to 30 min also indicates the continuous generation of nuclei to form AgNPs during the plasma process.

The DLS technique is used to determine the formation of AgNPs and their size distribution. It is found that the hydrodynamic diameter of FRU-AgNPs based on C3 operation for 30 min is in a range of 15 to 40 nm as shown in Figure 13. The mean and standard deviation of diameter are 25.3 and 5.8 nm, respectively. According to the DLS analysis, the polydispersity index (*PDI*) can be calculated by an equation of $PDI = \left(\frac{\sigma}{d}\right)^2$ where *d* is the mean diameter and σ is the standard deviation of diameter, the *PDI* value in this experiment equals to 0.05, which is less than 0.1 implying monodisperse nanoparticles [37].

3.5 Effect of AgNO_3 concentrations on FRU-AgNPs formation

Here, a relatively low concentration of AgNO_3 is defined in a range of 0.125 mM to 1 mM. Based on C3 operation, it can be observed that when the AgNO_3 concentration is increased, the intensity of the AgNPs solution color also gradually increases as shown in Figure 14. The higher intensity of the color is caused by the greater amount of Ag^+ supplied in the solution as expected. Ag^+ is converted to Ag^0 monomer for AgNP formation. Although plasma treatment time is quite as long as 30 minutes, the AgNP solutions prepared from 0.125, 0.25, 0.5 and 1 mM after plasma treatment are semi-transparent in color as shown in Figure 14. This is probably due to Ag^+ supplied in the solution being almost depleted for AgNP formation.

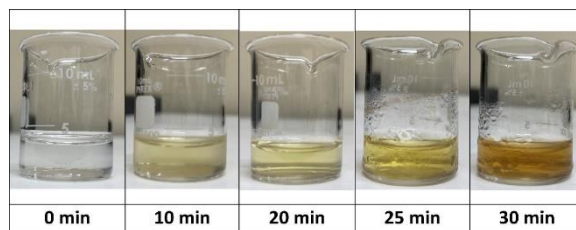


Figure 12: Photographs of AgNPs solution taken immediately after plasma treatment of 0, 10, 20, 25 and 30 min that are operated by C3 at 1 mM AgNO_3 and 40 mM fructose. A volume ratio of AgNO_3 to fructose and helium flow rate is fixed to be 2:1 mL and 0.4 LPM, respectively.

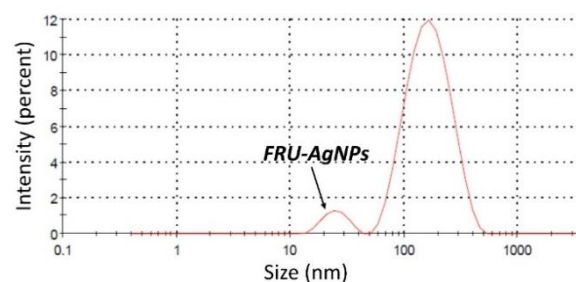


Figure 13: Size distribution by intensity profile obtained by dynamic light scattering (DLS) technique of silver nanoparticles. Experimental parameters are 1 mM AgNO_3 +40 mM fructose solution and 30 min of plasma treatment time on C3 operation. The volume ratio of AgNO_3 to fructose and helium flow rate are fixed to be 2:1 mL and 0.4 LPM, respectively.

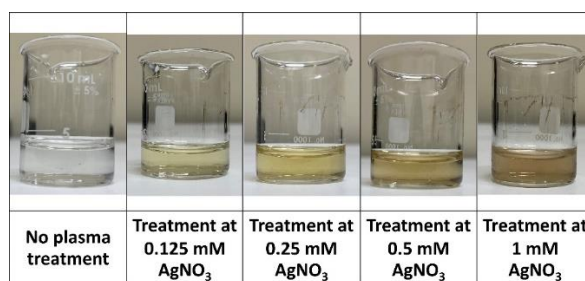


Figure 14: Photographs of AgNP solution taken immediately after plasma treatment on C3 operation for AgNO_3 concentrations of 0.125, 0.25, 0.5 and 1 mM stabilized by 40 mM fructose. A volume ratio of AgNO_3 to fructose and plasma treatment time is fixed to be 2:1 mL and 30 min, respectively.

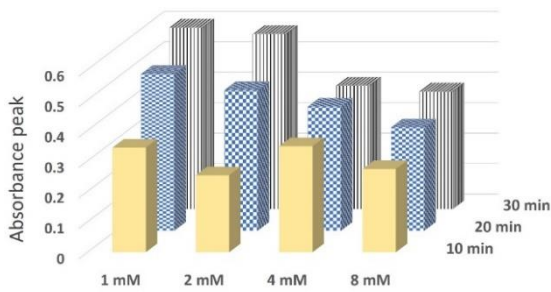


Figure 15: Three-dimensional bar graphs representing the relationships of AgNO₃ concentration and plasma treatment time to SPR absorbance peak. AgNO₃ concentrations of 1, 2, 4 and 8 mM are mixed with 40 mM fructose by 2:1 mL on C3 operation for plasma treatment times of 10, 20 and 30 min.

3.6 Effect of higher AgNO₃ concentrations and plasma treatment time on FRU-AgNPs formation

For further investigation on the effect of relatively higher concentration on AgNP synthesis, AgNO₃ concentrations of 1, 2, 4 and 8 mM are selected with plasma treatment times of 10, 20 and 30 min on C3 operation. In Figure 15, it can be clearly seen that an increase in plasma treatment time leads to an increase in absorbance peak (*abp*) for all concentrations used from 1 to 8 mM. However, the slopes of 1 mM and 2 mM AgNO₃ are greater than those of 4 mM and 8 mM AgNO₃. Moreover, when the plasma treatment time is fixed, the absorbance peak tends to decrease with an increase in AgNO₃ concentration, as obviously seen in the conditions of 20- and 30-min plasma treatment times as shown in Figure 15. This result can be explained by the theory of free energy for nucleation. Since free energy change (ΔG) required to form the nucleus before reaching stability can be evaluated from an equation of $\Delta G = 4\pi r^2\gamma + \frac{4}{3}\pi r^3\Delta G_v$ where r is the radius of the spherical nucleus, γ is surface energy, ΔG_v is free energy of the bulk crystal as well as critical radius of nucleus (r_{crit}) can be evaluated from an equation of $r_{crit} = \frac{-2\gamma}{\Delta G_v}$ as described more in detail in the literature [38]. When $r < r_{crit}$, the nucleus will shrink by redissolving into the solution, conversely when $r > r_{crit}$, the nucleus will continue to grow resulting in larger nanoparticles. Due to the constant power supply to generate plasma, the whole free energy (ΔG) brought from plasma species is also constant. Meanwhile, the groups of Ag⁰ monomers have equal possibility to receive free energy and form the nucleus.

So, in higher concentration of AgNO₃, the groups of Ag⁰ monomer are also high, meanwhile the free energy is conserved. This situation is more difficult to form the nucleus with $r > r_{crit}$ than the burst nucleation as proposed by LaMer [38] rarely happens, resulting in less AgNP formation (low *abp*). To evaluate the influences of AgNO₃ concentration and plasma treatment time on AgNP synthesis, the relationships of *abp* to concentration and treatment time are assumed to be linear regression in the ranges of 1–8 mM AgNO₃ and 10–30 min treatment time. After numerical calculation, a linear regression equation is obtained as $abp \sim 0.009t - 0.020con + 0.297$, where t = treatment time and con = concentration of AgNO₃. From this approximation, the slope of 0.020 is greater than that of 0.009. This suggests that concentration has more influence on AgNP synthesis than the treatment time in the scopes of 1–8 mM AgNO₃ and 10–30 min treatment time. Also, the optimal AgNO₃ concentration can be deduced in a range of 1–2 mM based on our plasma jet system and 40 mM fructose as a stabilizing solution. Interestingly, at 10 min treatment time, it is found that a decline of *abp* from 1 mM to 8 mM AgNO₃ is unclear and it fluctuates as shown in Figure 15. One explanation might be that below 10 min treatment time, free energy (ΔG) consumption is not mainly used on burst nucleation. It might be mainly used for creating the nanoparticles with $r < r_{crit}$ and partially converting to potential energy linking the fructose stabilizers to AgNP surfaces simultaneously even though multiple-burst nucleation can occur within 10 min.

3.7 Effect of fructose concentrations on FRU-AgNPs formation

Based on C3, to investigate the effect of fructose concentration on AgNP synthesis, fructose in aqueous solution of 5, 10, 20 and 40 mM are selected and mixed with 2 mM AgNO₃ by volume ratio of 1:2 mL, respectively. Under these concentrations and plasma treatment time fixed at 30 min, it is found that absorbance peak (*abp*) increases with increasing in concentration of fructose solution. The increase in fructose concentration results in a blue shift of UV-Vis absorption spectra from 419 nm (5 mM fructose) to 416 nm (40 mM fructose) (Figure 16), indicating the formation of smaller nanoparticles. This result is in good agreement with previous reports [39], [40]. It should be noted here that when molecules are close to metal nanoparticles, the binding energy could be formed.

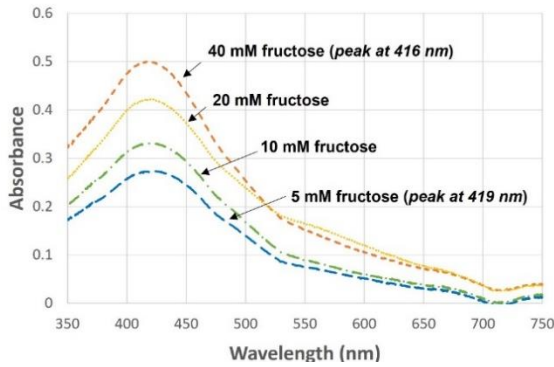


Figure 16: UV-Vis absorption spectra of AgNPs solution measured immediately after plasma treatment for 30 min. Fructose concentrations of 5, 10, 20 and 40 mM are mixed with 2 mM AgNO₃ by volume ratio of 1:2 mL on C3 operation.

The strength of that binding energy depends on each type of molecule [41]. As expected, the more fructose concentration is used, the more stabilizers are chemically bonded on the surface of the nanoparticles, obstructing further Ag⁰ monomers to grow on the surface and preventing aggregation. The Ag⁰ monomers which cannot be grown on the surface, might be used for further nucleation. Consequently, this leads to smaller AgNP sizes and higher concentrations of the AgNPs. In addition, in Figure 16, the absorbance peaks (*abp*) of 5, 10, 20 and 40 mM fructose are 0.27, 0.33, 0.41 and 0.5, respectively.

Hence, the ratios of *abp* as $\frac{abp_{f10}}{abp_{f5}}$, $\frac{abp_{f20}}{abp_{f10}}$ and $\frac{abp_{f40}}{abp_{f20}}$, would be 1.22, 1.24 and 1.22 respectively, where *abp_{f5}*, *abp_{f10}*, *abp_{f20}* and *abp_{f40}* denote the absorbance peaks from using 5, 10, 20 and 40 mM fructose, respectively. Significantly, these ratios are nearly the same value and can be approximated as 1.23 based on this experimental observation. Principally, *abp* is directly proportional to the number of AgNPs in solution (*n*) as *abp* ∝ *n*. Hence, it can be written as $\frac{abp_{f10}}{abp_{f5}} \sim \frac{n_{f10}}{n_{f5}}$ where *n_{f5}* and *n_{f10}* denote the number of AgNPs in solution from using 5 mM and 10 mM fructose, respectively. One can infer that by doubling the concentration of fructose, the number of AgNPs in solution will increase to about 1.23 times in an experimental range of 5–40 mM fructose.

It has been reported that the agglomerates can be found at a density of fructose less than 1 mM [42]. This might be interpreted that the density of fructose

molecules (*D_{fru}*) is insufficient to stabilize the solution. Thus, the concentration of fructose which is greater and not too far from 1 mM, can be assumed to vary directly proportional to free energy for fructose binding on the surfaces of silver nanoparticles. Hence, the equation of free energy for fructose stabilized silver nanoparticles (FRU-AgNPs) creation can be simply represented in Equation (1) as.

$$\Delta G_{FRU-AgNPs} = \Delta G_{s-AgNPs} + \Delta G_{v-AgNPs} + \Delta G_{fru} \quad (1)$$

Here, $\Delta G_{FRU-AgNPs}$ is defined as the total free energy received from plasma for fructose stabilized silver nanoparticle creation, $\Delta G_{s-AgNPs}$ is total free energy for creating the surfaces of silver nanoparticles and can be expressed as $\Delta G_s = n4\pi R^2\gamma$, where *R*, *n* and γ are the average radius, average number, and surface free energy of silver nanoparticles, respectively. $\Delta G_{v-AgNPs}$ is defined as the total free energy of the bulk crystal of a silver nanoparticle. ΔG_{fru} is total free energy for fructose binding on the surfaces of silver nanoparticles and it can be assumed and expressed as $\Delta G_{fru} \sim kD_{fru}$, where *k* and *D_{fru}* are variation constant and density of fructose in the solution. Nevertheless, for simplified approximation, it is assumed that the total free energy of the bulk crystal of silver nanoparticles will be released and subsequently used for fructose binding on the surfaces. Thus, $\Delta G_{v-AgNPs}$ can be combined with ΔG_{fru} to be $\Delta G'_{fru}$ represented in Equation (2) as.

$$\Delta G_{FRU-AgNPs} = \Delta G_{s-AgNPs} + \Delta G'_{fru} \quad (2)$$

$\Delta G'_{fru}$ is a certain amount of free energy partially received from plasma before completion of fructose binding or it can be roughly considered as a certain amount of free energy before merging with a term of $\Delta G_{v-AgNPs}$. Also, $\Delta G'_{fru}$ can be expressed as $\Delta G'_{fru} \sim k'D_{fru}$ where *k'* is arbitrary variation constant. Since, plasma generation power is conserved in this experiment, so $\Delta G_{FRU-AgNPs}$ is also conserved. From Equation (2), by substitutions of $\Delta G_{s-AgNPs}$ and $\Delta G'_{fru}$ for 5 and 10 mM fructose, the balanced equation can be obtained in Equation (3) as

$$n_{f5}(4\pi R_{f5}^2)\gamma + k'D_{fru5} = n_{f10}(4\pi R_{f10}^2)\gamma + k'(D_{fru10}) \quad (3)$$

In Equation (3), *R_{f5}* and *R_{f10}* denote the average radius of silver nanoparticles from using 5 mM

fructose and 10 mM fructose, respectively. D_{fru5} and D_{fru10} denote the density of fructose in solution from using 5 and 10 mM fructose, respectively. In Equation (3), by substitutions of $D_{fru10} = 2D_{fru5}$, $R_2 = aR_1$ where, a is arbitrary ratio between R_1 and R_2 and $\frac{n_{f10}}{n_{f5}} \sim 1.23$ then rearranging equation, the reduced form of Equation (3) can be expressed in Equation (4) as.

$$1 - 1.23a^2 = \frac{k'D_{fru5}}{n_{f5}(4\pi R_1^2)^{\gamma}} \quad (4)$$

From Equation (4), to consider about boundary condition of this equation by evaluating the value of a , a term of $1 - 1.23a^2$ must be greater than 0. Then solving an inequality of $1 - 1.23a^2 > 0$, it can be found that the positive value of a must stay in a range of 0 to 0.9 in order to validate Equation (4). From this approximation, it can be interpreted that by doubling the concentration of fructose in a range of 5 to 40 mM, the silver nanoparticle size would not exceed 0.9 times of its initial size. Additionally, in Equation (4), D_{fru5} or $\Delta D_{fru} = D_{fru10} - D_{fru5}$ is an independent variable and it might be an indicator of the value of a as, the lower density of fructose in solution, the greater value of a . Another meaning, it can be implied that when the density of fructose in the solution is less, the slope of AgNP size reduction is less than that of higher fructose density in the solution by taking reduction size < 0.9 times of initial size into account. However, this approximation might be useful for a modified study model and is required for further investigation. In (Figure 17) corresponding to the graphs in (Figure 16), a change in color from transparent to pale yellow for all fructose concentrations from 5 to 40 mM apparently confirms the formation of AgNPs.

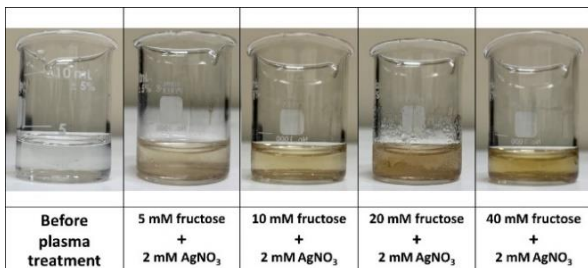


Figure 17: Photographs of AgNP solution taken immediately after plasma treatment for 30 min on C3. Fructose solutions of 5, 10, 20 and 40 mM are used as stabilizing solutions and mixed with 2 mM AgNO₃ by volume ratio of 1:2 mL.

The color intensity increases slightly with an increase in fructose concentration. This is probably due to the total free energy for the creation of silver nanoparticle surfaces as a term of $n(4\pi R^2)^{\gamma}$ does not reduce much even though the total free energy for fructose binding on silver nanoparticle surfaces is increased. It is also noted that a term of R^2 decreases due to more fructose molecules obstructing the growth process. Meanwhile, a term of n would be increased to preserve free energy for the creation of total surfaces of silver nanoparticles. These explanations for the reduction of AgNP size and increase in the number of AgNPs correspond to the graphs (Figure 16).

Although the relatively high concentration of fructose (40 mM) has more effectiveness, it helps to understand the relationship between yield of AgNPs and fructose concentration in this study. However, in the environmental aspect, fructose concentration could be reduced in a range of 1–5 mM and the yield or stability of AgNPs could be compensated by increasing plasma treatment time, increasing electrical power supply, or even mixing fructose with other low-cost stabilizing agents, e.g., some polysaccharides or polysaccharides from plant extract, respectively. In addition, this study shows that non-thermal atmospheric pressure plasma has the potential to synthesize AgNPs. The cost of production would be reduced if non-thermal atmospheric pressure plasma is generated from ambient air and the cost of production would mainly depend on electrical power.

3.8 Repeatability of the plasma treatment

In this study, the repeatability of the plasma treatment is simply determined by the absorbance peak from UV-Vis spectroscopy by using C3 configuration. It is found that the wavelengths at the absorbance peak of repeat numbers 1–5 are completely the same at 410 nm as shown in (Table3).

Table 3: Repeatability of C3 jet configurations, plasma treatment time and gas flow rate are fixed to be 20 minutes and 0.4 LPM, respectively.

Repeat Number / Experimental Results	Repeat Number				
	R1	R2	R3	R4	R5
Wavelength at absorbance peak (nm)	410	410	410	410	410
Absorbance peak	0.45	0.47	0.35	0.44	0.4

In addition, the average (mean) and standard deviation (SD) of the absorbance peak is 0.422 ± 0.048 . From this result, the absorbance peak from each repeat

number is slightly different (approximately SD/mean $\sim 10\%$). This slight difference might be due to the uncertainty of liquid circulation via magnetic stirring and gas flow controlled by mechanical rotameter etc. However, this difference is practically acceptable and can be improved for greater precision. Hence, plasma treatment has a repeatability and a feasibility for large-scale AgNP production.

3.9 Anti-bacterial activity of FRU-AgNPs against *Escherichia coli*

The inhibition activity of AgNPs is tested against Gram negative bacteria, *E. coli*. by disc diffusion assay. As a result, there are clear zones surrounding the filter paper (Figure 18), that previously AgNP solutions are dropped on. The clear zones indicate no bacteria growth in these areas. It is found that the inhibition zone of AgNPs is 8.87 ± 0.55 mm. Antibiotic streptomycin is also used as a positive control and shows an inhibition zone of 18.30 ± 0.62 mm (Figure 18).

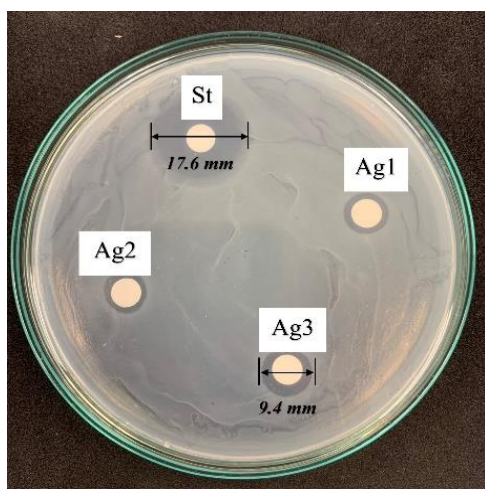


Figure 18: Disc diffusion assay of AgNPs against *E. coli*. The diameters of growth inhibition zone of AgNPs are 8.3, 8.9 and 9.4 mm as a symbol (Ag1), symbol (Ag2) and symbol (Ag3), respectively. Antibiotic streptomycin is used as a positive control. Those diameters of streptomycin are 17.6 as symbol (St), 18.8 and 18.5 mm.

Additionally, the MIC of AgNPs against *E. coli* is 3.125 mg/mL. The current experiment result is consistent with a study [13]. Several studies have proposed anti-bacterial mechanism of AgNPs against *E. coli*. It is believed that AgNPs attach to the bacterial cell wall and cell membrane, causing morphological

changes in cell walls and membranes and membrane detachment [23], [24]. AgNPs are found to increase the membrane charge from -28.5 ± 2.9 mV to -3.5 ± 0.8 mV, leading to an alteration of membrane permeability and cell death [43]. Moreover, the ROS and free radicals produced by AgNPs can cause oxidative stress in bacteria, in which they may disrupt the scavenging mechanisms of glutathione (GDH), which is a thiol group-containing substance responsible for antioxidant activity in cells, by directly binding with thiol groups in GSH, resulting in increased concentrations of ROS and free radicals. High concentrations of ROS and free radicals can damage mitochondrial membrane, proteins and DNA and subsequently cause cell death [43].

4 Conclusions

In this research, a non-thermal atmospheric pressure helium plasma jet is applied for AgNPs synthesis, the parameters as four types of plasma jet configuration (C1–C4), 10–30 min of plasma treatment times, 0.125–8 mM of AgNO_3 concentrations and 5–40 mM fructose concentrations are used for parameterization. It is found that the optimal conditions for AgNP synthesis are plasma jet configuration of C3, plasma treatment time of 30 min, AgNO_3 concentration of 1–2 mM, and fructose concentration of 40 mM. According to DLS analysis, the hydrodynamic sizes of AgNPs are found in a range of 15–40 nm with an average size of 25 nm that corresponds to the SPR absorbance peaks of UV-Vis spectra in a range of 400–420 nm. The filament-like discharge has more influence on AgNP synthesis than the fog-like discharge due to higher plasma electron flux entering the solution. In addition, the filament-like discharge just below the liquid precursor surface (C3) generates more solvated electrons than the one above the liquid precursor surface (C1) and results in the highest concentration of AgNPs. The AgNP concentration increases with the increase in plasma treatment time and AgNO_3 concentration. However, the condition for using AgNO_3 concentration is limited not to be greater than 1–2 mM. This limitation is probably due to the insufficient density of non-thermal atmospheric pressure plasma electrons. By using fructose concentration at 40 mM and AgNO_3 concentration less than 1 mM, AgNPs are well-stabilized over a period of 1 h after plasma treatment for all C1–C4. Moreover, it is found that an increase in fructose stabilizer concentration results in a slight increase in AgNP



concentration while its size becomes smaller. This synthesized AgNPs show anti-bacterial activity against *E. coli*. Therefore, the non-thermal atmospheric pressure plasma jet can be used to rapidly and eco-friendly synthesize AgNPs for biomedical and agricultural applications.

Acknowledgments

The authors would like to acknowledge Maejo University Phrae Campus for supporting facilities in this research. The authors also would like to acknowledge members of the Laboratory of Protein Engineering and Protein Bioinformatics, Department of Biochemistry, as well as members from Center of Nanotechnology, Department of Chemistry, Faculty of Science, Kasetsart University for equipment and technical support.

Author Contributions

J.S.: conceptualization, methodology, formal analysis, investigation, resources, data curation, writing-original draft, writing-review and editing, visualization, supervision and project administration; K.C.: methodology, formal analysis, investigation, writing original draft, writing-review and editing and visualization; L.T.: methodology, investigation and writing-original draft; C.S.: methodology, investigation and writing-original draft; K.C.: conceptualization, methodology, resources, writing-review and editing, supervision and project administration. All authors have read and agreed to the published version of the manuscript.

Conflicts of Interest

The authors declare no conflict of interest.

References

- [1] P. N. J. Arjun, B. Sankar, K. V. Shankar, N. V. Kulkarni, S. Sivasankaran, and B. Shankar, "Silver and silver nanoparticles for the potential treatment of COVID-19: A review," *Coating*, vol. 12, Nov. 2022, Art. no. 1679.
- [2] S. Khan, M. Zahoor, R. S. Khan, M. Ikram, and N. U. Islam, "The impact of silver nanoparticles on the growth of plants: The agriculture applications," *Heliyon*, vol. 9, Jun. 2023, Art. no. e16928.
- [3] P. Palani, H. Trilaksana, R. M. Sujatha, K. Kannan, S. Rajendran, K. Korniejenko, M. Nykiel, and M. Uthayakumar, "Silver nanoparticles for waste water management," *Molecules*, vol. 28, Apr. 2023, Art. no. 3520.
- [4] M. M. Martin and R. E. Sumayao Jr., "Facile green synthesis of silver nanoparticles using *Rubus rosifolius* Linn aqueous fruit extracts and its characterization," *Applied Science and Engineering Progress*, vol. 15, no. 3, Oct. 2021, Art. no. 5511, doi: 10.14416/j.asep.2021.10.011.
- [5] D. Chicea, A. Nicolae-Maranciuc, A. S. Doroshkevich, L. M. Chicea, and O. M. Ozkendir, "Comparative synthesis of silver nanoparticles: Evaluation of chemical reduction procedures, AFM and DLS size analysis," *Materials*, vol. 16, Jul. 2023, Art. no. 5244.
- [6] M. Momcilovic, J. Petrovic, M. Nemoda, J. Ciganovic, N. Krstulovic, M. Ognjanovic, and S. Zivkovic, "Laser ablation in water for silver and gold nanoparticle synthesis and their application for improvement of TEA CO₂ LIBS setup performance," *Applied Physics B*, vol. 129, Mar. 2023, Art. no. 62.
- [7] V. Darakai, C. Punsawad, J. Jitnonom, M. Nisoa, and P. Rattanakit, "Microwave-assisted ultrafine silver nanoparticle synthesis using *Mitragyna speciosa* for antimalarial applications," *De Gruyter*, vol. 13, no. 1, Mar. 2024, Art. no. 20230257.
- [8] T. R. Acharya, M. Jang, G. J. Lee, and E. H. Choi, "A comprehensive study on the synthesis, characteristics, and catalytic applications of submerged hydrogen-mixed argon plasma synthesized silver nanoparticles," *Current Applied Physics*, vol. 56, pp. 36–46, Oct. 2023.
- [9] M. H. Al-Janabi, C. Y. Ataol, and A. Ramizy, "Characterization of silver nanoparticles prepared by cold plasma reaction," *Iraqi Journal of Applied Physics*, vol. 20, no. 2A, pp. 279–284, Apr. 2024.
- [10] H. K. Tawfeeq, N. K. Abdalameer, R. H. Jassim, and M. M. Shehab, "Silver nanoparticles synthesized by cold plasma as an antibiofilm agent against *Staphylococcus epidermis* isolated from acne," *Nano Biomedicine and Engineering*, vol. 16, pp. 101–109, Mar. 2024.
- [11] M. Shepida, O. Kuntiyi, Y. Sukhatskiy, A. Mazur, and M. Sozanskyi, "Microplasma synthesis of antibacterial active silver nanoparticles in sodium polyacrylate solutions,"

- Bioinorganic Chemistry and Applications*, vol. 2021, Oct. 2021, no. 4465363.
- [12] L. Chandana, P. Ghosal, T. Shashidhar, and Ch. Subrahmanyam, "Enhanced photocatalytic and antibacterial activity of plasma-reduced silver nanoparticles," *Royal Society of Chemistry Advances*, vol. 8, pp. 24827–24835, Jul. 2018.
- [13] J. Weerasinghe, W. Li, R. Zhou, R. Zhou, A. Gissibl, P. Sonar, R. Speight, K. Vasilev and K. K. Ostrikov, "Bactericidal silver nanoparticles by atmospheric pressure solution plasma processing," *Nanomaterials*, vol. 10, May 2020, Art. no. 874.
- [14] K. Yambe, T. Izumida, I. Ohyama, and H. Akatsuka, "Comparison of electron densities and temperatures in helium and argon nonthermal atmospheric-pressure plasmas by continuum spectral analysis," *IEEE Transactions on Plasma Science*, vol. 52, no. 2, pp. 384–394, Feb. 2024.
- [15] T. N. Tran, C. H. Oh, and W. Lee, "Determination of electron properties of a helium atmospheric pressure plasma jet with a grounded metallic target," *Plasma Processes and Polymers*, vol. 18, Dec. 2021, Art. no. e2100092.
- [16] J. Sornsakdanuphap, P. Suanpoot, Y. J. Hong, B. Ghimire, G. Cho, H. S. Uhm, D. Kim, Y. J. Kim, and E. H. Choi, "Electron temperature and density of non-thermal atmospheric pressure argon plasma jet by convective wave packet model," *Journal of the Korean Physical Society*, vol. 70, no. 11, Jun. 2017.
- [17] D. Amir, R. R. Nasaruddin, N. S. Engliman, S. Sulaiman and M. S. Mastuli, "Effect of stabilizers in the synthesis of silver nanoparticles and methylene blue oxidation," in *6th International Conference on Biotechnology Engineering*, vol. 1192, 2021, Art. no. 012031.
- [18] V. Kulikouskaya, K. Hileuskaya, A. Kraskouski, I. Kozerozhets, E. Stepanova, I. Kuzminski, L. You, and V. Agabekov, "Chitosan-capped silver nanoparticles: A comprehensive study of polymer molecular weight effect on the reaction kinetic, physicochemical properties, and synergistic antibacterial potential," *SPE Polymers*, vol. 3, pp. 77–90, Jan. 2022.
- [19] M. A. Taher, E. Khojah, M. S. Darwish, E. A. Elsherbiny, A. A. Elawady, and D. H. Dawood, "Biosynthesis of silver nanoparticles by polysaccharide of *Leucaena leucocephala* seeds and their anticancer, antifungal properties and as preservative of composite milk sample," *Journal of Nanomaterials*, vol. 2022, Jan. 2022, Art. no. 7490221.
- [20] A. Dzimitrowicz, A. Motyka-Pomagruk, P. Cyganowski, W. Babinska, D. Terefinko, P. Jamroz, E. Lojkowska, P. Pohl, and W. Sledz, "Antibacterial activity of fructose-stabilized silver nanoparticles produced by direct current atmospheric pressure glow discharge towards quarantine pests," *Nanomaterials*, vol. 8, no. 10, p. 751, Sep. 2018.
- [21] H. Yin, M. Zhou, X. Chen, T. F. Wan, L. Jin, S. S. Rao, Y. J. Tan, R. Duan, Y. Zhang, Z. X. Wang, Y. Y. Wang, Z. H. He, M. J. Luo, X. K. Hu, Y. Wang, W. Y. Situ, S. Y. Tang, W. E. Liu, C. Y. Chen, and H. Xie, "Fructose-coated Ångstrom silver prevents sepsis by killing bacteria and attenuating bacterial toxin-induced injuries," *Theranostics*, vol. 11, pp. 8152–8171, Jul. 2021.
- [22] N. Mammari, E. Lamouroux, A. Boudier, and R. E. Duval, "Current knowledge on the oxidative-stress-mediated antimicrobial properties of metal-based nanoparticles," *Microorganisms*, vol. 10, no. 2, p. 437, Feb. 2022.
- [23] X. Yan, B. He, L. Liu, G. Qu, J. Shi, L. Hu, and G. Jiang, "Antibacterial mechanism of silver nanoparticles in *Pseudomonas aeruginosa*: proteomics approach," *Metallomics*, vol. 10, pp. 557–564, Mar. 2018.
- [24] P. R. More, S. Pandit, A. D. Filippis, G. Franci, I. Mijakovic, and M. Galdiero, "Silver nanoparticles: Bactericidal and mechanistic approach against drug resistant pathogens," *Microorganisms*, vol. 11, no. 2, p. 369, Feb. 2023.
- [25] C. Corbella, S. Portal, and M. Keidar, "Flexible cold atmospheric plasma jet sources," *Plasma*, vol. 6, pp. 72–88, Feb. 2023.
- [26] F. Liu, M. Cai, B. Zhang, Z. Fang, C. Jiang, and K. K. Ostrikov, "Hydrophobic surface modification of polymethyl methacrylate by two-dimensional plasma jet array at atmospheric pressure," *Journal of Vacuum Science & Technology A*, vol. 36, Oct. 2018, Art. no. 061302.
- [27] M. D. Teli, K. K. Samanta, P. Pandit, S. Basak and S. K. Chattopadhyay, "Low-temperature dyeing of silk fabric atmospheric pressure helium/nitrogen plasma," *Fiber and Polymers*, vol. 16, no. 11, pp. 2375–2383, Nov. 2015.
- [28] R. Zaplotnik, M. Biscan, D. Popovic, M. Mozetic, and S. Milosevic, "Metastable helium atom density in a single electrode atmospheric



- plasma jet during sample treatment,” *Plasma Sources Science and Technology*, vol. 25, May 2016, Art. no. 035023.
- [29] S. Yallappa, J. Manjanna, S. K. Peethambar, A. N. Rajeshwara, and N. D. Satyanarayan, “Green synthesis of silver nanoparticles using *Acacia farnesiana* (sweet acacia) seed extract under microwave irradiation and their biological assessment,” *Journal of Cluster Science*, vol. 24, pp. 1081–1092, Jun. 2013.
- [30] A. Karatutlu, A. Barhoum, and A. Sapelkin, “Theories of nanoparticle and nanostructure formation in liquid phase,” in *Emerging Applications of Nanoparticles and Architecture Nanostructures*. Amsterdam, Netherlands: Elsevier, pp. 597–619, 2018, doi: 10.1016/b978-0-323-51254-1.00020-8.
- [31] B. Dong, N. Xue, G. Mu, M. Wang, Z. Xiao, L. Dai, Z. Wang, D. Huang, H. Qian, and W. Chen, “Synthesis of monodisperse spherical AgNPs by ultrasound-intensified Lee-Meisel method, and quick evaluation via machine learning,” *Ultrasonics Sonochemistry*, vol. 73, Feb. 2021, Art. no. 105485.
- [32] V. S. Santosh, K. Kondeti, U. Gangal, S. Yatom, and P. J. Bruggeman, “Ag⁺ reduction and silver nanoparticle synthesis at the plasma–liquid interface by an RF driven atmospheric pressure plasma jet: Mechanisms and the effect of surfactant,” *Journal of Vacuum Science and Technology A*, vol. 35, Jul. 2017, Art. no. 061302.
- [33] M. Adamowska, B. Pałuba, and W. Hyk, “Electrochemical determination of nanoparticle size: Combined theoretical and experimental study for matrixless silver nanoparticles,” *Molecules*, vol. 27, Apr. 2022, Art. no. 2592.
- [34] H. Wang, R. Han, M. Yuan, Y. Li, Z. Yu, P. J. Cullen, Q. Du, Y. Yang, and J. Wang, “Evaluation of plasma-activated water: Efficacy, stability, physicochemical properties, and mechanism of inactivation against *Escherichia coli*,” *LWT-Food Science and Technology*, vol. 184, Jun. 2023, Art. no. 114969.
- [35] X. Yang, C. Zhang, Q. Li, and J. H. Cheng, “Physicochemical properties of plasma-activated water and its control effects on the quality of strawberries,” *Molecules*, vol. 28, Mar. 2023, Art. no. 2677.
- [36] P. Traiwacharanon, K. Timsorn, and C. Wongchoosuk, “Flexible room-temperature resistive humidity sensor based on silver nanoparticles,” *Materials Research Express*, vol. 4, Aug. 2017, Art. no. 085038.
- [37] N. Raval, R. Maheshwari, D. Kalyane, S. R. Youngren-Ortiz, M. B. Chougule and R. K. Tekade, “Importance of physicochemical characterization of nanoparticles in pharmaceutical product development,” in *Basic Fundamentals of Drug Delivery*. Massachusetts: Academic Press, pp. 370–400, 2019, doi: 10.1016/B978-0-12-817909-3.00010-8.
- [38] N. T. K. Thanh, N. Maclean, and S. Mahiddine, “Mechanisms of nucleation and growth of nanoparticles in solution,” *Chemical Review*, vol. 114, pp. 7610–7630, Jul. 2014.
- [39] H. M. Yasin, W. Ahmed, A. Ali, A. S. Bhatti, and N. U. Rehman, “Micro-plasma assisted synthesis of multifunctional D-fructose coated silver nanoparticles,” *Materials Research Express*, vol. 6, Sep. 2019, Art. no. 1050a2.
- [40] A. J. González FÁ, A. Juan, and M. S. D. Nezio, “Synthesis and characterization of silver nanoparticles prepared with honey: The role of carbohydrates,” *Analytical Letters*, vol. 50, pp. 877–888, Apr. 2017.
- [41] H. T. Phan and A. J. Haes, “What does nanoparticles stability mean?,” *Journal of Physical Chemistry C: Nanomaterials and Interfaces*, vol. 123, no. 27, pp. 16495–16507, Dec. 2019.
- [42] U. Shuaib, T. Hussain, R. Ahmad, M. Zakaullah, F. E. Mubarik, S. T. Muntaha, and S. Ashraf, “Plasma-liquid synthesis of silver nanoparticles and their antibacterial and antifungal applications,” *Materials Research Express*, vol. 7, Mar. 2020, Art. no. 035015.
- [43] S. Tang and J. Zheng, “Antibacterial activity of silver nanoparticles: Structural effects,” *Advanced Healthcare Materials*, vol. 7, May 2018, Art. no. e1701503.